Biological Thermal Detection: Micromechanical and Microthermal Properties of Biological Infrared Receptors

V. Gorbunov,[†,‡] N. Fuchigami,[†] M. Stone,[§] M. Grace,[||] and V. V. Tsukruk*,[†]

*Department of Materials Science & Engineering, Iowa State University, Ames, Iowa 50011,
TM Microscopes, Sunnyvale, California 94089, Materials and Manufacturing Directorate, Air Force
Research Laboratory/MLPJ, Wright-Patterson Air Force Base, Ohio 45433, and Department of Biological
Sciences, Florida Institute of Technology, Melbourne, Florida 32901*

Bioinspired design of biomimetic sensors relies upon the complete understanding of properties and functioning of biological analogues in conjunction with an understanding of their microstructural organization at various length scales. In the spirit of this approach, the microscopic properties of infrared (IR) receptors of snakes with "infrared vision" were studied with scanning thermal microscopy and micromechanical analysis. Low surface thermal conductivity of 0.11 W/(m K) was measured for the IR receptor surfaces as compared to the nonspecific skin areas. This difference in surface thermal conductivity should result in a significant local temperature gradient around the receptor areas. Micromechanical analysis showed that pit organs were more compliant than surrounding skin areas with an elastic modulus close to 40 MPa. In addition, the maximum elastic modulus was detected for the outermost layer with gradually reduced elastic resistance for the interior. The porous microstructure of the underlying tissue combined with the highly branched microfibrillar network (*Biomacromolecules* **2001**, *2*, 757) is thought to be responsible for such a combination of biomaterial properties. Considering these biomaterials features, we postulated a possible design of an artificial photothermal detector inspired by the microstructure of natural receptors. This bioinspired design would include a microfabricated cavity filled with an ordered lattice of microspheres with a gradient periodicity from the surface to the interior. Such a "photonic cavity" could provide an opportunity for multiple scattering at wavelength tuned to $8-12$ μm as a range of highest sensitivity.

Introduction

The bioinspired principles of the sophisticated design of prospective artificial sensors composed of "soft" matter, such as macromolecular and organic materials, can be an efficient way toward a new generation of microsensors. The bioinspired design of biomimetic sensors necessitates the complete understanding of biological functional properties in conjunction with their microstructural organization at various length scales. Comprehensive studies of such multiscale structural organization ranging from single biomacromolecules through cellular and tissue-level organization should be conducted concurrently with testing of their properties and functioning. From this prospective, highly sensitive infrared (IR) detection observed in some snakes attracts significant interest.[1−9]

In the spirit of this approach, we focused on determining the microstructural design and the combination of biomaterials properties necessary for artificial thermal sensors composed of organic/polymeric materials. In the first part of this communication (see ref 9), we reported the results of microstructural studies of IR biological receptors without addressing their ultimate thermal properties. In this communication, we address the question of the microscopic properties of these receptors and discuss how their peculiarities can be related to microstructural organization discussed earlier.

The ability of certain snakes to perform IR imaging is well-documented.[1−6] Microstructural studies showed a distinctive surface morphology on their IR receptors with a characteristic nanopit array.[5,7−9] The average spacing of the nanopit array (about 500 nm) observed within the receptor surface areas was suggested to play a critical role in selective IR adsorption. This value is close to the grating spacing required for efficient reflection of electromagnetic radiation characteristic for sunlight without affecting IR absorbance.[9] The efficiency of reflection of incoming radiation with this surface grating should be highest in the range close to the maximum emmitance of natural sun/moon light. This can effectively reduce overheating of the receptor areas and make them functional under conditions of high thermal background. Future models of artificial IR sensors based upon this design should include this surface feature, whose dimensions provide selectivity over the electromagnetic spectral range.

It is clear that the effective transmission of thermal stimuli requires unique thermal properties of the receptor surface.[10] However, these properties remain untested. In this com-

* To whom correspondence should be addressed, vladimir@iastate.edu.
† Iowa State University.
‡ Thermomicroscopes.
§ Air Force Research Laboratory.
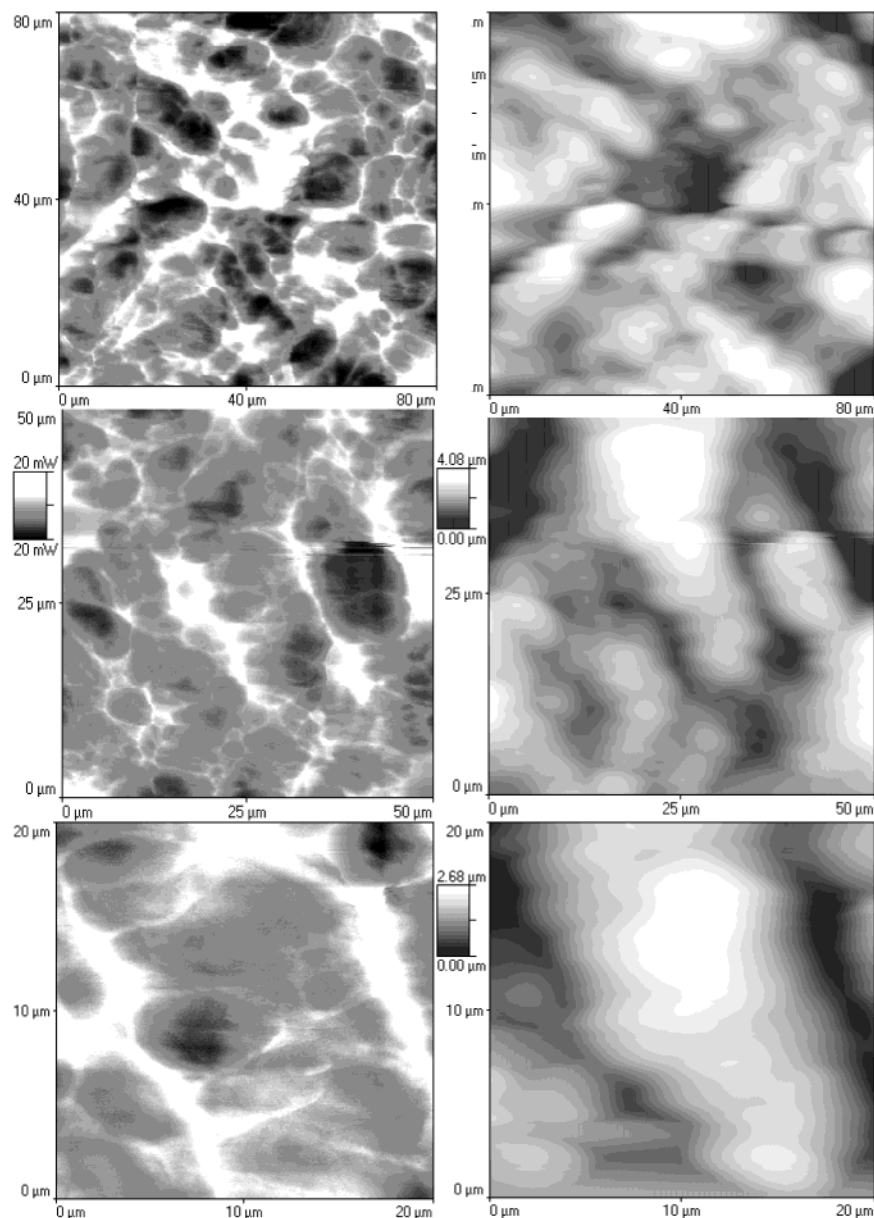|| Florida Institute of Technology.

Figure 1. Topography (right) and surface distribution of heat dissipation (left) for formaldehyde-treated pit organ surface of Ball python at three different magnifications.

munication, we focus on comparative studies of micromechanical and microthermal properties of IR receptors. Here, we report on the microthermal and micromechanical properties of snake IR receptors of living and chemically treated snake tissues analyzed by the application of scanning thermal microscopy (SThM) and micromechanical analysis (MMA). SThM and MMA techniques were introduced several years ago and are widely used for the characterization of compliant materials.[11−17] These techniques were modified and further developed in our laboratory for the quantitative microprobing of surface microthermal conductivity and micromechanical properties of compliant materials such as polymers and biomaterials.[18−25] These techniques allow for the direct microprobing of surface microthermal and micromechanical properties with sub-micrometer resolution.

Here we discuss how important elements of both tissue and cellular-scale microstructural organization can provide effective photothermal functioning of these IR receptors. Finally, we suggest a prospective model of a thermooptical

cavity that depicts the main photothermal properties of biological receptors.

Several major questions were addressed in the course of this study:

Do surface thermal conductivity and micromechanics distinguish snake IR receptor organs from nonspecific skin areas?

Can their micromechanical and microthermal properties be related to photothermal mechanism of IR reception?

What type of microstructural organization, at tissue and cellular levels, is responsible for unique properties of IR receptors?

How can these properties aid in the design of bioinspired photothermal IR detectors based upon macromolecular materials?

Experimental Section

We studied both living tissue close to in vivo conditions and formaldehyde-fixed tissue of two different types of
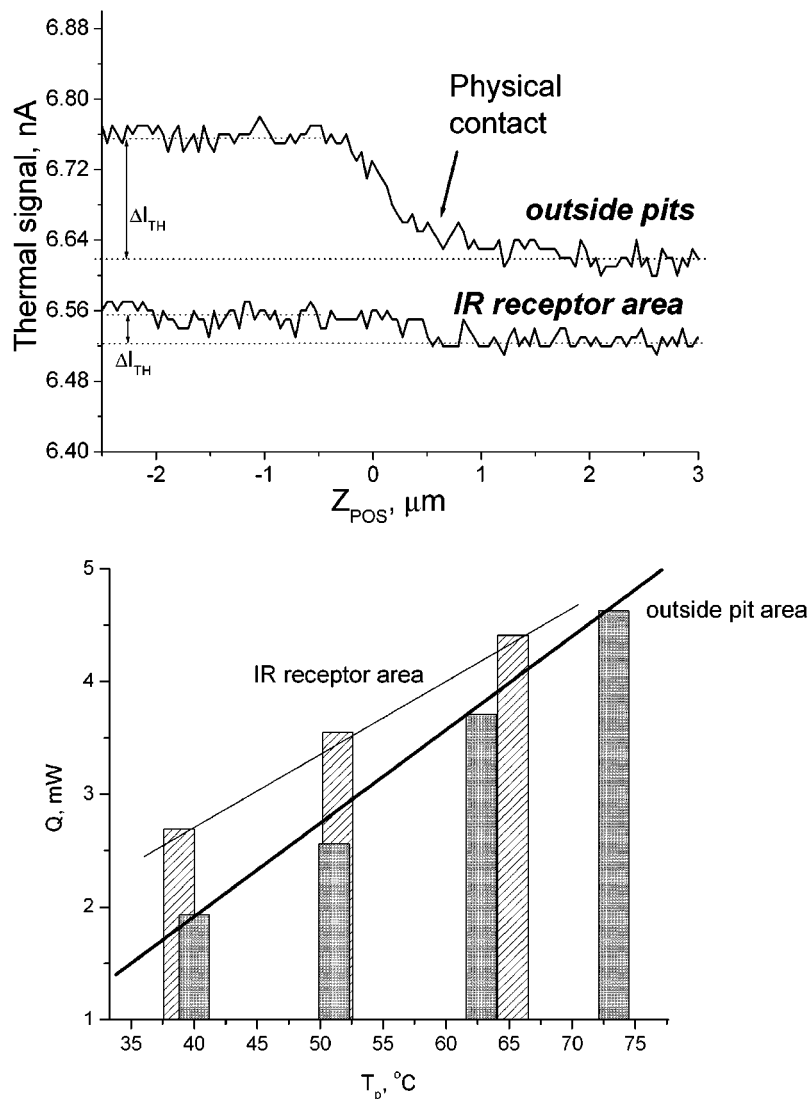
Figure 2. Heat dissipation as the thermal probe approaches the surface of the pit organ receptor and an area outside the pit organ (top). Heat dissipation at physical contact at different initial temperature differences between thermal probe and surface for pit organ and nonpit organ snake skin areas (bottom). The absolute value of thermal signal is in relative units that greatly depends on tip parameters and applied voltage.

Table 1. Micromechanical (elastic modulus) and Microthermal (surface thermal conductivity) Properties of Receptor Organ Surfaces and Nonspecific Skin Areas for Living and Treated Tissues

	IR receptor organ	nonspecific skin area
thermal conductivity (W/(m K))[a]		
Burmese python (living tissue)	N/A	N/A
Ball python (formaldehyde-treated tissue)	0.11 ± 0.03	0.34 ± 0.05
polyurethane[b]	0.15	
glass[b]	1.6	
polyethylene[b]	0.37	
Young's modulus (MPa)[c]		
Burmese python (living tissue)	39 ± 16	144 ± 117
Ball python (formaldehyde-treated tissue)	43 ± 21	154 ± 33

[a] Mean and standard deviations are provided, averaged over 3 locations, 15 probings total. [b] Data are taken from ref 19. [c] Mean and standard deviations are provided, averaged over three locations, 1024 probings in each location.

snakes with IR imaging capabilities (Table 1). Both specimens were studied under instant wet conditions provided by a specially designed sample holder mounted on a scanning stage.[9] Details of sample preparation were described earlier.[9] Briefly, for preliminary studies, we used formaldehyde-fixed tissue from ball python with pit organs isolated with a razor

blade and placed in a wet holder to prevent skin drying. Living tissue was obtained from Burmese python. The snake was deeply anesthetized by inhalation anesthesia (Metofane) and euthanized by cervical dislocation. Pit organs and other tissues were quickly dissected and held in oxygenated reptilian physiological Ringer's solution. Under these conditions, tissues were able to survive for up to several days. Multiple scanning of a single specimen took several hours with a continuous supply of fresh physiological Ringer's solution. Samples for investigation were placed on a concave glass support covered by a wet towel with its edges submerged in an aqueous bath to provide local 100% humid environment during measurements. Liquid absorbed by the towel formed a thin water layer on an open surface area available for scanning probe microscopy (SPM). SPM scanning was performed on living tissue specimens within several hours after mounting to ensure a nondegraded state of the surface.

Microthermal imaging was done in the SThM mode on an Explorer microscope (Thermomicroscopes). Microthermal probing of surface thermal conductivity was done with
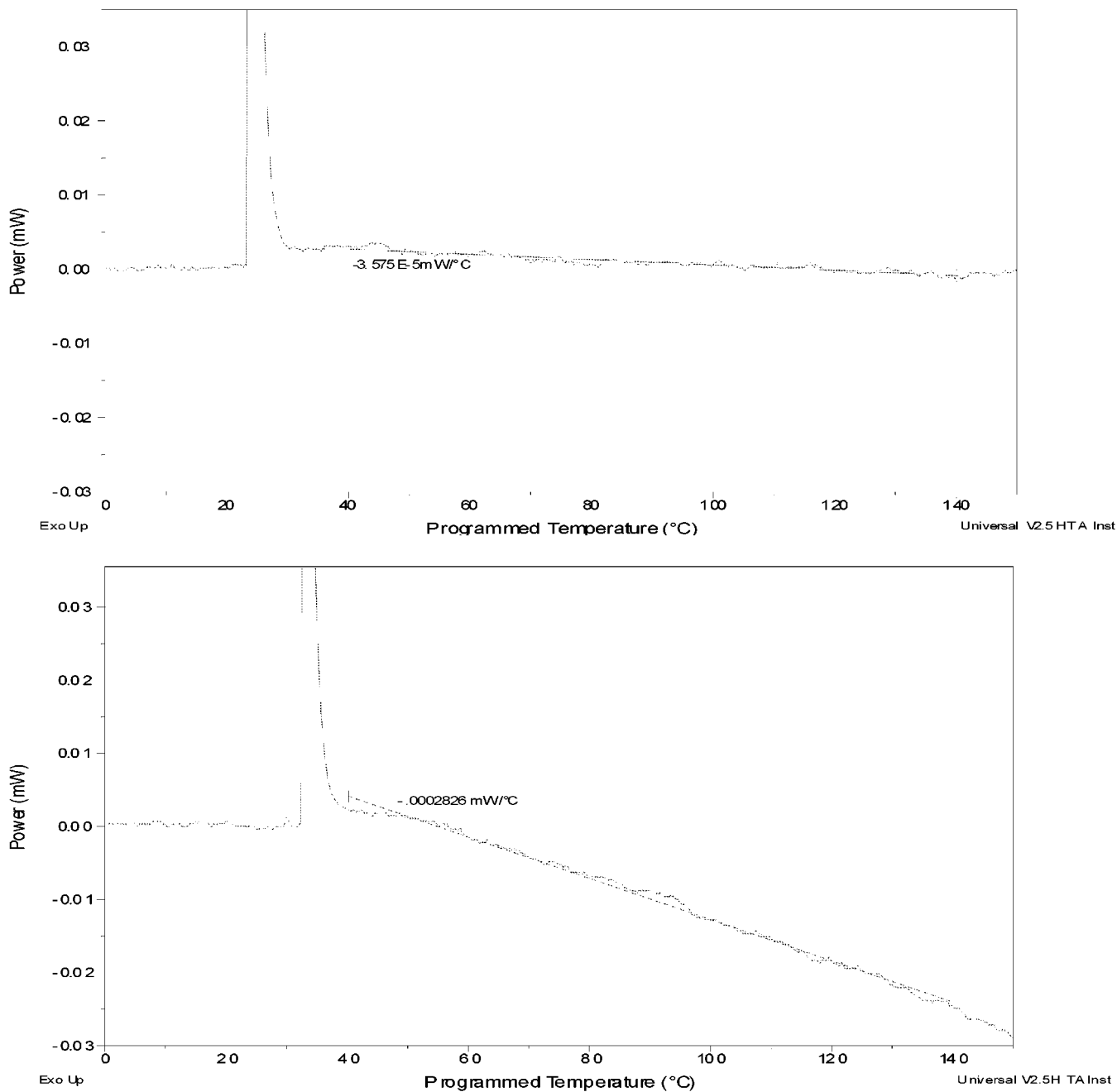
Figure 3. Heat dissipation of the thermal probe at the point of contact during a heating cycle for the pit organ receptor (top) and for nonspecific snake skin areas (bottom). Strong peaks correspond to electronic feedback response at room temperature. The absolute value of the thermal signal is in relative units that depend strongly on tip parameters and applied voltage.

microthermoanalysis (μTMA) and microthermal probing (μTP) modes.[19,26] We measured thermal dissipation of the thermal probe in the proximity of snake skin under two different scenarios. First, as the preheated thermal probe was brought close to the surface, heat dissipation was monitored. Thermal signal–distance data allowed calculation of heat dissipation before, during, and after actual physical contact of the thermal tip and the surface and, thus, variation of heat dissipation associated with physical contact (μTP technique). Second, the temperature of the thermal probe was raised after direct physical contact with the skin surface and the heat dissipation was monitored during the heating cycle (μTA technique). Experimental data were analyzed according to methods described earlier.[18–20]

MMA of receptor surface properties was performed on a Dimension 3000 microscope according to the experimental procedure described in detail elsewhere.[21–25] Surface areas of several micrometers across were probed in the force–volume regime with lateral resolution in the range of 30–200 nm. Histograms of the surface distribution of elastic modulus were obtained by processing an array of force–distance curves using Hertzian contact mechanics approximation of the elastic deformation. Experimental data were collected under completely elastic conditions (full recovery of surface deformation) as force–distance measurements and converted to surface deformation–normal load data. Depth profiling of mechanical responses was obtained using a
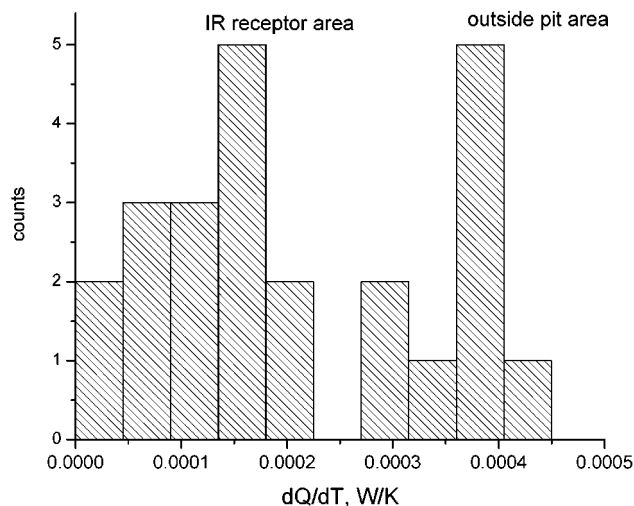
Figure 4. Histograms of surface distribution of thermal conductivities across receptor surface areas and outside pit receptor area.

double-spring model with variable spring coefficients according to the procedure described in refs 21 and 22.

Results and Discussion

Microthermal Properties. Testing of the microthermal properties of snake skin involved several independent experiments. First, we scanned receptor organ surfaces with the SThM technique to determine whether any singularities in the surface thermal conductivity associated with pit structure could be observed (Figure 1). For all surface areas, we observed a very uneven distribution of heat dissipation in local areas (several micrometers across) and this variation was on the order of several microwatts. Comparison of surface topography with the heat dissipation distribution showed a close correlation between these parameters. Shallow areas displayed higher heat dissipation while raised areas showed much lower local heat dissipation. This suggested that the observed uneven surface distribution of the heat dissipation was caused mainly by topographical contribution.[26] Variable surface topography leads to variable contact area between the thermal tip and the surface, and thus, variable integrated heat transfer at the contact point. At high magnification (scan size 20 × 20 μm), regular changes in the surface distribution of heat dissipation were observed (Figure 1). This may be attributed to the terrace-like surface morphology as was discussed in ref 9.

Scanning at higher magnification was constrained by the limited spatial resolution of our current SThM setup. The radius of heat dissipation distribution under probing conditions can reach 10 μm.[20] Spatial resolution of the thermal probe for compliant materials was estimated to be within 0.5−1 μm,[18] which is too low to resolve the nanopit array with the diameter of a single nanopit below 300 nm.[5−9] This estimation sets the limits of lateral resolution of the microthermal probing and the depth of its thermal sensing under given experimental conditions. Considering that a snake pit organ is several millimeters in diameter and neuronal receptor terminals are located several micrometers below the receptor surface, we conclude that we measured integrated lateral
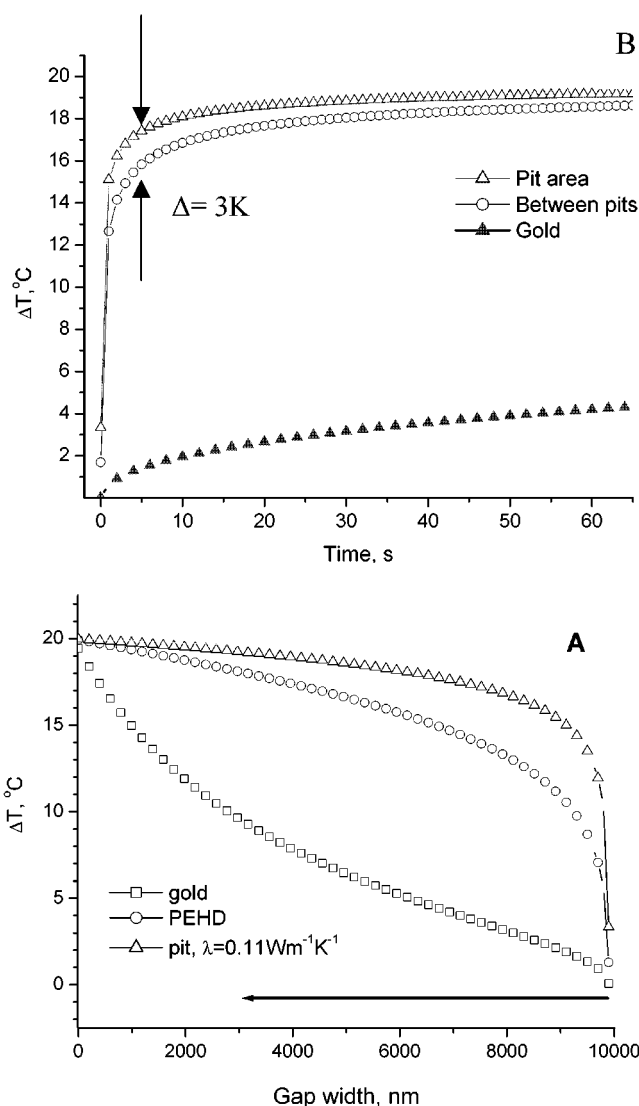

Figure 5. Simulation of surface temperature variation beneath the thermal tip under different conditions: (a) the thermal tip approaching surfaces with low and high thermal conductivity in comparison with pit receptor areas; (b) surface temperature for pit organ receptors, outside receptor areas, and gold surfaces for a stationary thermal tip positioned 10 μm above the surface with the tip temperature of 40 °C initiated at $t = 0$.

microthermal responses of the pit organ surface as well as features within a thin (several micrometer) layer beneath this surface. The probing area was very small in comparison to total pit organ size; thus, the influence of adjacent nonspecific skin areas (outside the pit organ) was unlikely.

To estimate the absolute value of the surface thermal conductivity, we exploited two different approaches described in detail previously.[20,26] The first approach included the measurement of heat dissipation, ΔQ, at the physical contact between the thermal probe preheated to temperature T_p and the snake skin surface with an initial temperature T_s. The second approach relied on the instant monitoring of heat dissipation $Q(T)$ at the contact point after tip engagement during temperature increase. The quasi-steady-state model of heat transfer between a pointlike heat source and a planar surface predicted a linear relationship between temperature-normalized heat dissipation within the contact area of radius

R_c and surface thermal conductivity, λ, in the form[18,26]

$$\Delta Q/\Delta T = k\lambda R_c \qquad (1)$$

where k is a proportionality factor, which depends on geometry and mechanics at the contact point. This equation is valid for hemispherical thermal sources and a relatively slow variation of temperature and position of the thermal source. This was the case for our experimental setup as has been discussed in detail earlier.[19−21]

We found that heat dissipation, ΔQ, increased after physical contact of the thermal tip with the snake skin surface (Figure 2). This increase was much higher for the pit organ surface than for nonpit surface areas. Repetition of such probing using different initial tip temperatures showed a virtually linear correlation with ΔT as expected from eq 1 (Figure 2). A different temperature dependence of the heat dissipation was measured for pit organ and nonpit skin with direct physical contact between tip and the skin surface (Figure 3). This slope provided an independent evaluation of the surface thermal conductivity. Both independent approaches applied here gave similar results on thermal conductivity and will be discussed below.

The cumulative results of multiple probing of the micro-thermal properties of receptor and nonspecific areas (up to 30 independent measurements) are presented in Figure 4. The surface distribution of the surface thermal conductivity showed a broad distribution with two distinctive maxima separated far beyond random variations. The value for pit organ receptor areas was much lower than those obtained for the surface areas outside of the snake receptor organs. The absolute value of surface thermal conductivity was calculated according to the procedure described earlier.[19] We obtained absolute values of thermal conductivity of $\lambda = 0.11$ W/(m K) for the pit organ surface and $\lambda = 0.34$ W/(m K) for the nonspecific skin areas outside of the pit organs but in close proximity (Table 1). The latter value is close to the typical values for organic carbon-based macromolecular materials such as polyethelene.[19] On the other hand, the surface thermal conductivity of the pit organ receptor area is lower than typical values for the vast majority of organic materials (0.15−0.4 W/(m K)) (Table 1).[19,20]

Therefore, the major conclusion from our microthermal measurements is that snake IR-receptive pit organs possess surface thermal conductivity lower than surrounding non-specific skin areas. To understand the implications of these results for thermal sensing, we conducted simulations of surface temperature variation for pit organ and nonpit organ surfaces in the presence of a thermal source above the surface. For these simulations, we used the model of quasi-steady-state heat transfer adapted to SThM measurements in our previous publication.[20] For these calculations, we assumed published values for water as the heat capacity and density of snake tissue.[27]

We simulated thermal conductivity by analyzing surface temperature variation as the thermal probe approached the surface from an initial distance of 10 μm (Figure 5a). We observed a rapid increase in surface temperature as the probe approached the surface with pit receptor thermal properties. The surface temperature reached the initial temperature of
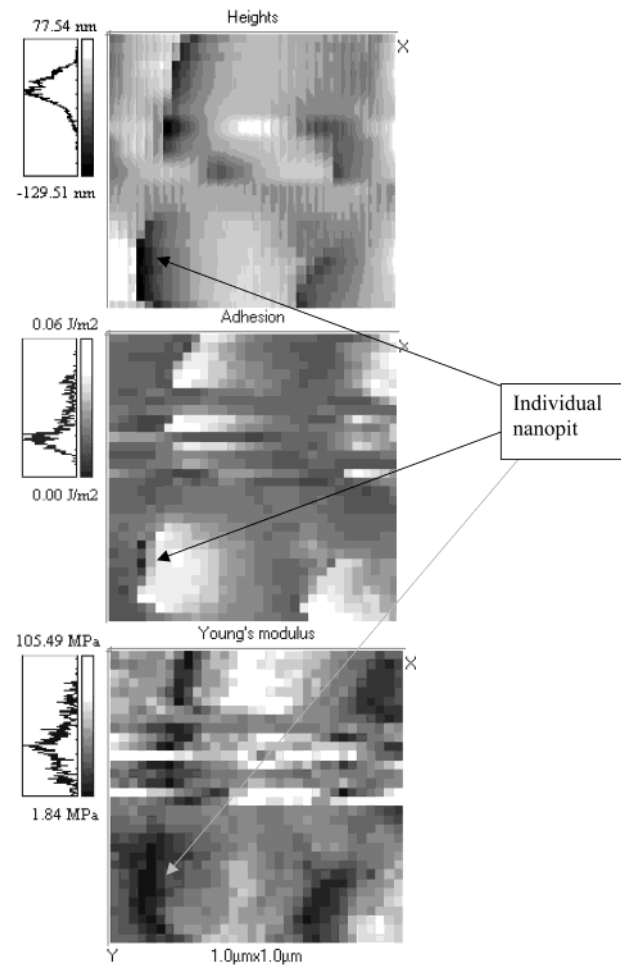

Figure 6. Micromapping of micromechanical surface properties of receptor surface areas containing nanopits obtained with 32 × 32 pixel resolution for the 1 × 1 μm area of living skin: surface topography (top), adhesive forces (middle), and elastic modulus (bottom). Left charts show histograms of surface distribution and vertical scales. Random horizontal lines are scanning instabilities.

the thermal tip at distances around 5 μm for an initial difference in temperatures of 20 °C. In contrast, the surface temperature of the areas outside the pit organ receptors rose at a slower pace similar to conventional macromolecular materials (Figure 5a). Finally, the surface temperature of a highly conductive material, such as gold, increased at a very slow rate under similar conditions (Figure 5a).

In addition, we simulated temperature variation on the surface beneath a stationary thermal probe located above the surface after its temperature was turned on (Figure 5b). These simulations demonstrated that the low thermal conductivity of pit receptors prevented rapid heat dissipation from the surface area with these characteristics and, therefore, caused rapid local temperature rise. The result was a significant temperature gradient between receptor and nonreceptor areas that can reach 3 °C for an initial temperature difference between the thermal probe and the surface of 20 °C (Figure 5b). As we observed, if the stationary thermal source was turned on far from the skin surface, a surface temperature gradient between receptor area and surrounding nonspecific skin areas was established immediately. The temperature difference reached 3 °C within several seconds and persisted over a long time period before thermal equilibration took
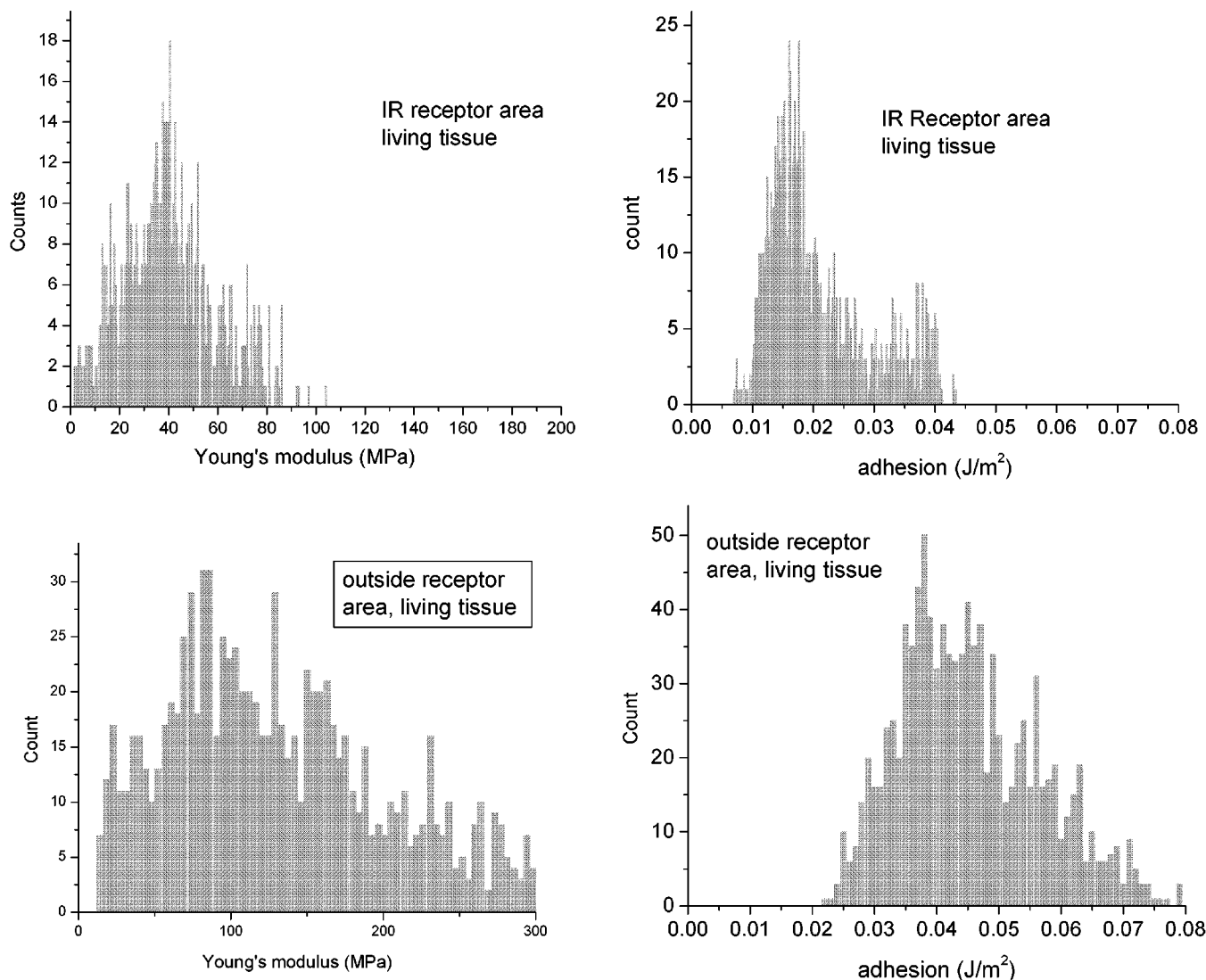
Figure 7. Histograms of the surface distribution of elastic moduli and adhesive forces inside the pit receptor and outside of the receptor areas for living tissue collected within 1 μm × 1 μm surface area.

place (at $t > 100$ s, Figure 5). This behavior was very different from that observed for surfaces of materials with high thermal conductivity (such as gold) where a much slower surface temperature rise is caused by high thermal diffusivity (Figure 5b).

Micromechanical Properties. To compare the micromechanical properties of pit organ receptor areas and non-specific skin areas, we probed the surface compliance (elastic response) of living tissues at different locations. We collected multiple force−distance curves (32 × 32 locations within 10 × 10 μm and 1 × 1 μm areas) and estimated elastic modulus from the repulsive part of these curves using a Hertzian contact mechanics model.[21] This allowed micro-mapping of the surface elastic properties with sub-micrometer spatial resolution and determination of elastic modulus values of 1 MPa to 10 GPa.[21] An example, shown in Figure 6, demonstrates concurrently obtained surface topography, surface distribution of adhesive forces, and elastic moduli for the pit organ receptor surface obtained at the highest resolution. These data clearly show that the shallow areas of nanopits (slightly deformed under indentation) correlate

with lower elastic modulus and much higher forces (the same areas are marked by arrows).

The surface distribution of elastic moduli and adhesive forces showed 40% standard deviation over different areas of a given sample due to random variations and different contributions from curved surface areas (Figure 7). Even so, a clear difference can be seen between the distributions of elastic responses of the pit organ surface and regions outside the pit organs. The surface distribution of Young's modulus values was broader and shifted toward higher values in areas outside the pit organs (Figure 7). This distribution was much sharper for pit organ tissue, and the average value of the elastic modulus was much smaller for these areas (39 MPa versus 144 MPa for the outside pit receptor area, Table 1). Both values were close to the elastic moduli obtained under similar conditions for formaldehyde-fixed ball python samples analyzed under wet conditions (Table 1). The value for regions outside of the pit organs is typical for tough plastics, while the elastic modulus for receptor areas resembles that of more compliant materials such as highly cross-linked
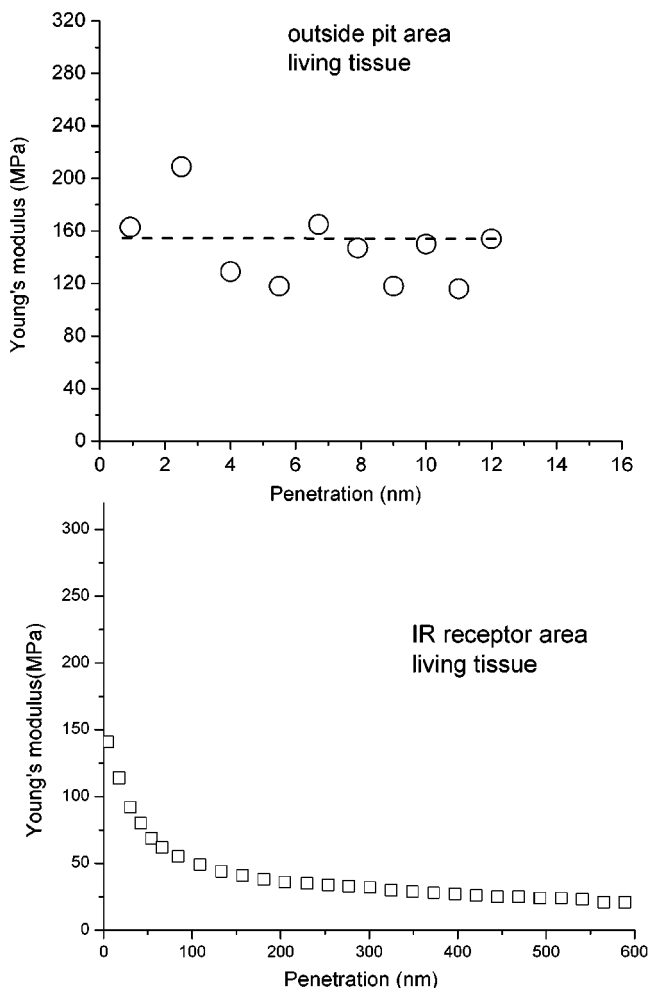
Figure 8. Depth gradient of elastic modulus for pit organ surface (bottom) and for nonpit organ areas (top) of living tissue. Note very different penetration scales for the two plots.

rubbers.[21] Adhesive forces were detected to be much lower for receptor surface areas (Figure 7).

An elastic modulus, calculated from force–distance data at different penetration depths, provides information about the presence of depth gradients in micromechanical response. Typical data for nonspecific skin and receptor areas are presented in Figure 8. It is clear from these data that micromechanical properties of pit receptors areas were very different from those of nonspecific skin areas. First, skin outside the receptor areas showed virtually no gradient of elastic modulus. Under normal given load, elastic penetration did not exceed 15 nm due to a limited spring constant value of the cantilever used. The absolute value of elastic modulus was about 140 MPa for all indentation depths (Figure 8). In contrast, receptor surface areas were much more compliant and could be elastically deformed with the same cantilever up to 1–2 μm (Figure 8). The depth of indentation was technically limited to 2–3 μm because of the maximum tip height of the atomic force microscope (AFM) cantilevers. Moreover, the elastic modulus for the receptor areas showed a significant depth gradient. A stiffer surface layer with a more compliant underlying material (with the elastic modulus below 20 MPa) was observed for these areas (Figure 8). These results indicate compliant, spongelike elastic behavior of pit receptor surfaces from living tissue allowing extremely

large reversible deformations under modest normal loads. Higher initial stiffness likely represents properties of the outermost cornified surface layer.[7]

Therefore, the major conclusion of micromechanical testing is that the surface material in the infrared pit organ receptor areas is much more compliant than that outside the receptor areas and the pit organ possesses a significant micromechanical depth gradient with a stiffer surface layer and a more elastic (compliant) interior. The combination of materials properties observed for pit organ receptor areas can be associated with the microstructure of the underlying tissue with a developed microporous organization as was discussed in part 1 (ref 9). This micropore, micro-foam-like tissue structure explains the high compliance of the pit receptor areas in comparison to the noncompliant nature of nonpit organ surface areas.

Discussion and Models

Combined measurements of micromechanical and microthermal properties and analysis of tissue microstructure revealed a much higher compliance and a lower surface thermal conductivity in the IR receptor surface areas compared to nonspecific skin areas in the vicinity of snake receptors. We suggest that the observed differences in microthermal and micromechanical properties are caused by the foamlike microstructure and high microporosity of tissue within the receptor areas. This porosity can be caused by the bundled microfibrillar structure as revealed by SPM studies in part 1 of this communication (ref 9) and presented in the model of pit receptors from the microstructural viewpoint in Figure 9. Here, inserts are AFM images of different receptor regions obtained with sub-micrometer resolution as discussed in detail in ref 9.

The first type of cellular microstructure depicted in this figure was observed at deeper levels (several micrometers).[9] It is composed of collagen-based microfibrils approximately 100 nm in diameter, with a regular periodicity of 68 nm along the fibril axis (Figure 9). These parameters are very close to values known for collagen microfibrils.[18] On the other hand, the highly developed cellular morphology observed in proximity to the surface represents the endings of nerve fibrils (Figure 9). The level of porosity estimated from the SPM images is within 30–60% for various locations and the pores possess a wide distribution of sizes with the average value about or below 1 μm. Additionally, Young's modulus of the surrounding tissue indicates a hard material that protects the integrity of the pit-based IR receptor.

From this consideration of underlying microstructural organization, we can interpret the peculiar surface properties of IR receptors and speculate on their role for functioning as IR sensors. From the standpoint of microthermal properties, air-filled surface microvoids with low thermal conductivity (λ_{air} is an order of magnitude lower than any organic material) in close proximity to the surface should significantly reduce the overall thermal conductivity of the pit receptors. Low surface thermal conductivity provides a significant reduction in heat dissipation from receptor areas, resulting in the fast rising of local surface temperature within
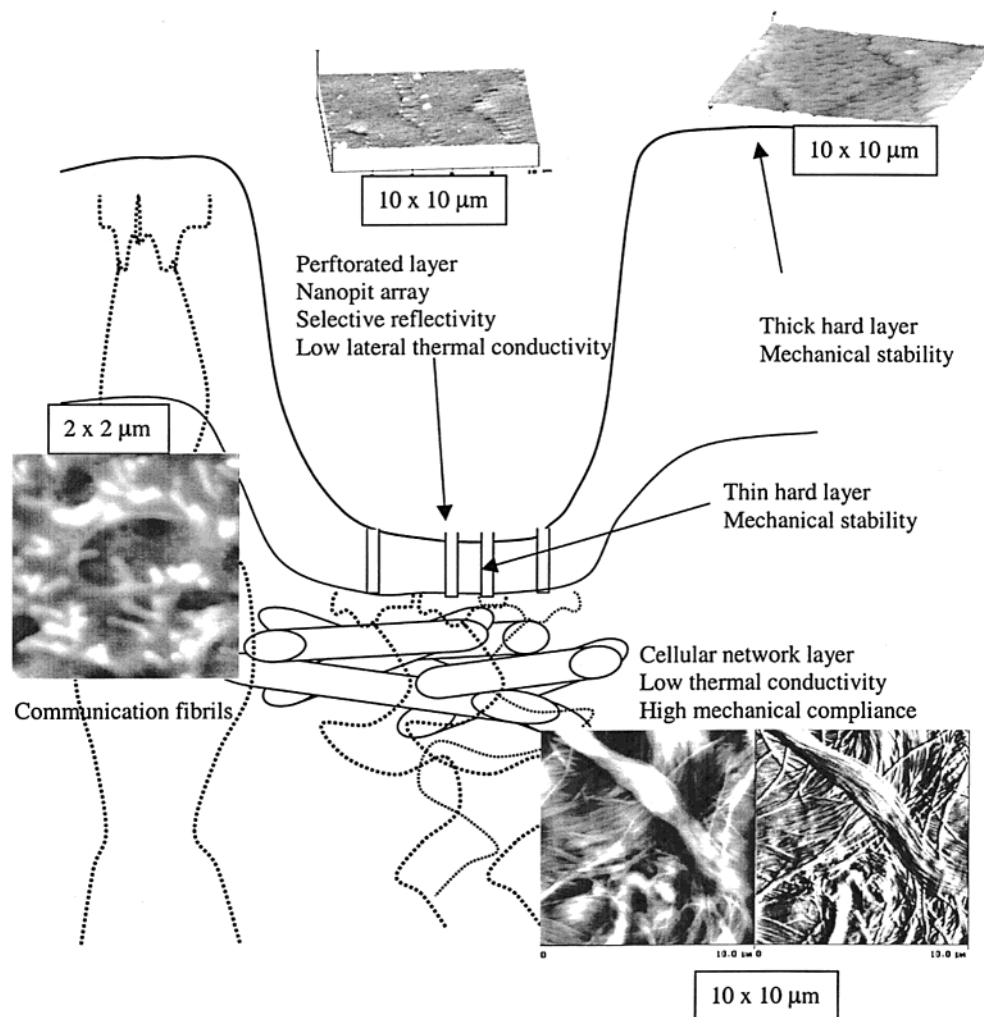
Figure 9. Sketch of the microstructure of the pit receptor organ from a materials perspective showing the major elements responsible for peculiar micromechanical and microthermal properties. A combination of microstructural results is taken from ref 9 and the present publication. Images represent AFM scans of various organ areas and reveal cell-level peculiarities of microstructural organization directly related to their localized properties. All images are SPM topography except topography and phase for right, bottom images.

the pit surface areas. In contrast, the neighboring nonspecific skin areas with higher thermal conductivity dissipate thermal energy faster and, thus, do not experience a similar rapid rise in localized surface temperature. This difference in heat dissipation processes gives rise to a temperature gradient between receptor and neighboring nonspecific skin areas. This temperature gradient combined with the close proximity of terminal nerve masses to the skin surface should provide an efficient mechanism for high-sensitivity photothermal detection. Thus, we suggest that the array of nanopits on the pit organ receptor surfaces may reduce effective surface thermal conductivity (reducing spatial heat dissipation) in addition to their function as a selective optical filter as was suggested earlier.[5-7] We believe that a similar mechanism of heat detection exists in other types of snakes such as Crotaline snakes, where a thin free-suspended membrane forms an air-filled cavity, separated from the bottom of the receptor by an air reservoir with very low thermal conductivity.[5]

Low thermal conductivity may also play a role in the spatial resolution of the receptors. The snake pit receptor is an imaging sensory organ used to target an infrared-emitting prey moving in three-dimensional space and is composed

of an array of individual sensory nerve terminals located beneath the receptor surface. Low lateral surface thermal conductivity should enhance spatial resolution by hindering the rate of thermal transfer between adjacent receptor terminal units.

Considering the major biomaterials features that enable the snake IR receptor organs to operate as a photothermal detector, we can postulate on the possible design of an artificial photothermal detector inspired by the microstructure of natural receptors (Figure 10). This bioinspired design includes several of the major elements discussed above. First, a microfabricated cavity is coated with multilayer films composed of densely packed hollow microspheres to create a thermally insulating layer isolating the thermally sensitive area. Second, this "thermal cavity" is filled with an ordered lattice of polymer microspheres with gradient periodicity from the surface to the interior. Such a "photonic cavity" could provide an opportunity for multiple scattering at wavelengths that correlate with internal periodicities (tuned to $8-12$ μm as a range of interest[10]). For example, microspheres with appropriate diameters can be composed of polymeric materials with strong adsorption bands in the range of $8-12$ μm. Multiple scattering along with strong adsorption
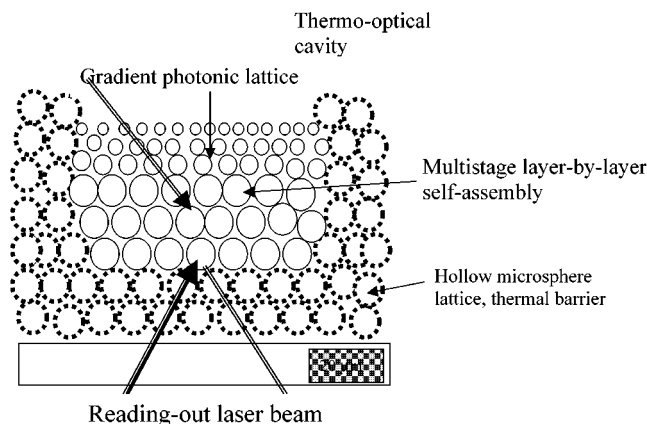
Figure 10. A model of the bioinspired design of a photothermal detector based on the principles of a thermooptical (thermophotonic) cavity composed of macromolecular materials self-assembled in an organized lattice. Bar represents approximate scale.

and thermal isolation should enhance the thermal response, i.e., enhance thermal expansion. A read-out laser detection scheme could be used to obtain information about average periodicity within this "thermophotonic" cavity. The use of a "chopper wheel" to impart a frequency to incoming thermal flux can be considered a means for periodic "refreshment" of thermal equilibrium to separate the influence of random thermal fluctuations and increasing thermal signature upon the detector.

This suggested design of a thermophotonic cavity as an efficient artificial thermal detector is feasible and can be achieved by a combination of modern self-assembling microfabrication techniques. Layer-by-layer self-assembly of polymer microspheres and weakly charged macromolecules with appropriate surface functionalities have been used for the wet chemistry fabrication of this type of microstructure.[28–30] Polymers with strong adsorption in the range of 8−12 μm are available for the fabrication of such microstructures and various organized photonic structures have been built.[31] Finally, for well-ordered lattices, a periodicity variation as small as 0.01% can be readily detected using a laser reflection or SPM-based detection scheme.

References and Notes

(1) Terashima, S.; Zhu, A.-Q. *Cell. Mol. Neurobiol.* **1997**, *17*, 195.

(2) Amemiya, F.; Goris, R. C.; Atobe, Y.; Ishii, N.; Kusunoki, T. *Anim. Eye Res.* **1996**, *15*, 13.

(3) Amemiya, F.; Ushuki, T.; Goris, R. C.; Kusunoki, T. *Anat. Rec.* **1996**, *246*, 135.

(4) Amemiya, F.; Goris, R. C.; Masuda, Y.; Kishida, R.; Atobe, Y.; Ishii, N.; Kusunoki, T. *Biomed. Res.* **1996**, *16*, 411.

(5) *Infrared Receptors and the Trigeminal Sensory System*; Terashima, S., Goris, R. C., Eds.; Harwood Academic Publishers: Amsterdam, 1998.

(6) Grace, M. S.; Woodward, O. M.; Church, D. R.; Calisch, G. *Behav. Brain Res.* **2001**, *119*, 23.

(7) Campbell, A. L.; Bunning, T.; Stone, M. O.; Church, D.; Grace, M. *J. Struct. Biol.* **1999**, *126*, 105.

(8) Hazel, J.; Stone, M.; Grace, M. S.; Tsukruk, V. V. *J. Biomechanics* **1999**, *32*, 477.

(9) Fuchigami, N.; Hazel, J.; Gorbunov, V.; Stone, M.; Grace, M.; Tsukruk, V. V. *Biomacromolecules* **2001**, *2*, 304.

(10) Jones, B. S.; Lynn, W. F.; Stone, M. O. *J. Theor. Biol.* **2001**, *209*, 201.

(11) Hammiche, A.; Reading, M.; Pollock, H. M.; Song, M.; Hourston, D. J. *Rev. Sci. Instrum.* **1996**, *67*, 4268.

(12) Pollock, H. M.; Hammiche, A.; Song, M.; Hourston, D. J.; Reading, M. *J. Adhes.* **1998**, *67*, 217.

(13) Hues, S.; Colton, R. J.; Meyer, E.; Guntherodt, H.-J. *MRS Bull.* **1993**, *1*, 41.

(14) Sarid, D. *Scanning Force Microscopy*; Oxford University Press: New York, 1991.

(15) Hazel, J.; Fuchigami, N.; Gorbunov, V.; Schmitz, H.; Stone, M.; Tsukruk, V. V. *Biomacromolecules* **2001**, *2*, 304.

(16) *Scanning Probe Microscopy in Polymers*; Ratner, B., Tsukruk, V. V., Eds.; ACS Symposium Series 694; American Chemical Society: Washington, DC, 1998.

(17) Tsukruk, V. V. *Rubber Chem. Technol.* **1997**, *70* (3), 430.

(18) Gorbunov, V. V.; Fuchigami, N.; Hazel, J. L.; Tsukruk, V. V. *Langmuir* **1999**, *15*, 8340.

(19) Gorbunov, V. V.; Fuchigami, N.; Tsukruk, V. V. *Probe Microsc.* **2000**, *2*, 53.

(20) Gorbunov, V. V.; Fuchigami, N.; Tsukruk, V. V. *Probe Microsc.* **2000**, *2*, 65.

(21) Chizhik, S. A.; Huang, Z.; Gorbunov, V. V.; Myshkin, N. K.; Tsukruk, V. V. *Langmuir* **1998**, *14*, 2606.

(22) Tsukruk, V. V.; Huang, Z. *Polym.* **2000**, *41*, 5541.

(23) Tsukruk, V. V.; Huang, Z.; Chizhik, S. A.; Gorbunov, V. V. *J. Mater. Sci.* **1998**, *33*, 4905.

(24) Tsukruk, V. V.; Gorbunov, V. V. *Probe Microsc.*, submitted.

(25) Tsukruk, V. V.; Gorbunov, V. V. *Microsc. Today* **2001**, *01−1*, 8.

(26) Pollock, H. M.; Hammiche, A. *J. Appl. Phys.* **2001**, *34*, 23.

(27) 27*Handbook of Chemistry and Physics*; Lide, D., Ed.; CRC: Boca Ratan, FL, 1995.

(28) Lvov, Yu. M.; Decher, G. *Cryst. Rep.* **1994**, *39*, 628.

(29) Bliznyuk, V. N.; Campbell, A.; Tsukruk, V. V. *Thin Organic Films*; Frank, C. W., Ed.; ACS Symposium Series 695; American Chemical Society: Washington, DC, 1998; p 220.

(30) Jiang, H.; Su, W.; Hazel, J.; Grant, J. T.; Tsukruk, V. V.; Cooper, T. M.; Bunning, T. J. *Thin Solid Films* **2000**, *372*, 85.

(31) Tsukruk, V. V. *Prog. Polym. Sci.* **1997**, *22*, 247.